

AUTOMATIC DEFORMATION OF RIEMANN–HILBERT PROBLEMS WITH APPLICATIONS TO THE PAINLEVÉ II TRANSCENDENTS

GEORG WECHSLBERGER AND FOLKMAR BORNEMANN

ABSTRACT. The stability and convergence rate of Olver’s collocation method for the numerical solution of Riemann–Hilbert problems (RHPs) is known to depend very sensitively on the particular choice of contours used as data of the RHP. By *manually* performing contour deformations that proved to be successful in the asymptotic analysis of RHPs, such as the method of nonlinear steepest descent, the numerical method can basically be preconditioned, making it asymptotically stable. In this paper, however, we will show that most of these preconditioning deformations, including lensing, can be addressed in an *automatic*, completely algorithmic fashion that would turn the numerical method into a black-box solver. To this end, the preconditioning of RHPs is recast as a discrete, graph-based optimization problem: the deformed contours are obtained as a system of shortest paths within a planar graph weighted by the relative strength of the jump matrices. The algorithm is illustrated for the RHP representing the Painlevé II transcendents.

1. INTRODUCTION

Remarkably many integrable problems in mathematics, mathematical physics, and applied mathematics can be cast as Riemann–Hilbert problems (RHPs): classical orthogonal polynomials and special functions, Painlevé transcendents, nonlinear PDEs related to the inverse scattering transform, and distributions in random matrix theory as well as in random combinatorial problems, to name just a few (Its 2003). A fruitful point of view is that RHPs generalize the representation of classical special functions by contour integrals; like these they have extensively been used in establishing deep asymptotic results such as connection formulae for the Painlevé transcendents (Fokas, Its, Kapaev and Novokshenov 2006). Here, a fundamental tool is the *method of nonlinear steepest descent*, which was introduced by Deift and Zhou (1993) to the asymptotic analysis of oscillatory RHPs.

Only quite recently, starting with a novel direct spectral collocation method of Olver (2011), RHPs have become the subject of study in numerical analysis. It turned out that the stability of this numerical method and its approximation properties strongly depends on matching most of the steps from the asymptotic analysis of the problem at hand: “One can expect that whenever the method of nonlinear steepest descent produces an asymptotic formula, the numerical method can be made asymptotically stable” (Olver and Trogdon 2012, p. 2). This way, the method is kind of *hybrid*: only after manually performing a series of expert analytic steps to deform the given RHP into another, equivalent, one, the thus “preconditioned” RHP is taken as input to the numerical algorithm. Hence, the

use of this numerical method has been limited so far to an audience that would have competent operational access to such a kind of expert knowledge.

In this paper we will give a *proof of concept* that most, if not all, of these deformations (at least if they were meant to stabilize the numerical method) can be addressed with an automatic, completely algorithmic approach that would turn the numerical method into a black-box solver for the user. Following Bornemann and Wechsberger (2012), who dealt with similar problems for contour integrals, we will recast the preconditioning of RHPs as a discrete, graph-based optimization problem: the desired deformation corresponds to a system of shortest paths within a weighted planar graph. Though we are not able, at this stage of our study, to determine the precise complexity class of this particular discrete optimization problem (NP-hard, polynomial, etc.) or to prove that our polynomial greedy algorithm would approximate the optimum within a certain range (which would be sufficient for the purpose of preconditioning), we will demonstrate for the example of the Painlevé II transcendents that, first, it will improve the stability of the input RHP significantly by several orders of magnitude and that, second, the resulting deformations of the RHP closely match what people have obtained by applying the method of nonlinear steepest descent.

Riemann–Hilbert problems. To fix the notation, we consider RHPs for a given oriented contour Γ , which is a finite union of simple smooth curves Γ_j ($j = 1, \dots, k$) in \mathbb{C} . By removing the finitely many points of self-intersection from Γ we obtain $\Gamma^0 \subset \Gamma$. Given a matrix-valued jump function $G : \Gamma^0 \rightarrow \text{GL}(m, \mathbb{C})$, the RHP determines a holomorphic function $\Phi : \mathbb{C} \setminus \Gamma \rightarrow \text{GL}(m, \mathbb{C})$ satisfying¹

$$\begin{aligned}\Phi^+(z) &= \Phi^-(z)G(z) & (z \in \Gamma^0), \\ \Phi(\infty) &= I.\end{aligned}$$

Here, $\Phi^\pm(z)$ denotes the non-tangential limit of $\Phi(z')$ as $z' \rightarrow z$ from the positive (negative) side of the contour. Existence and uniqueness of a solution Φ can be shown under some appropriate smoothness and decay assumptions on the jump function G (Deift 1999). To simplify the discussion of contour deformations, we assume that there are entire functions $G_j : \mathbb{C} \rightarrow \text{GL}(m, \mathbb{C})$ that continue the jump data G given on the part Γ_j of the contour Γ :

$$G|_{\Gamma^0 \cap \Gamma_j} = G_j|_{\Gamma^0 \cap \Gamma_j}.$$

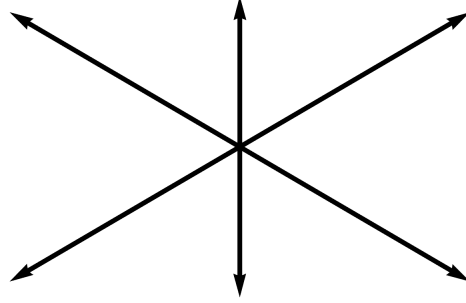
We consider the pairs (Γ_j, G_j) ($j = 1, \dots, k$) as the data of the RHP. Most often one is not interested in the full solution $\Phi(z)$ of the RHP but only on some derived quantities at ∞ , e.g., the residue

$$\text{res}_{z=\infty} \Phi(z) = \lim_{z \rightarrow \infty} z(I - \Phi(z)).$$

Example: Painlevé II. Throughout this paper we will illustrate our ideas for the RHP representing the Painlevé II equation

$$u_{xx} = xu + 2u^3.$$

¹The second condition is meant to imply that Φ has a holomorphic continuation at ∞ .

FIGURE 1. The six rays Γ_j of the RHP representing Painlevé II.

The general solution $u(x) = u(x; s_1, s_2)$ of this second-order ODE in the complex domain will depend on two independent complex parameters s_1 and s_2 , which are fixed in the following setup of the RHP: with the six rays (see Fig. 1)

$$\Gamma_j = \{s e^{i\pi(2j-1)/6} : s \geq 0\} \quad (j = 1, \dots, 6),$$

parameters s_j ($j = 1, \dots, 6$) interrelated by

$$s_1 - s_2 + s_3 + s_1 s_2 s_3 = 0, \quad s_4 = -s_1, \quad s_5 = -s_2, \quad s_6 = -s_3,$$

and the jump matrices

$$G_j(z) = \begin{cases} \begin{pmatrix} 1 & s_j e^{-\theta(z)} \\ 0 & 1 \end{pmatrix} & j \text{ even,} \\ \begin{pmatrix} 1 & 0 \\ s_j e^{+\theta(z)} & 1 \end{pmatrix} & j \text{ odd,} \end{cases}$$

with the phase function

$$\theta(z) = \frac{8i}{3} z^3 + 2ixz$$

the solution Φ of the RHP yields

$$u(x; s_1, s_2) = -2 \operatorname{res}_{z=\infty} \Phi_{1,2}(z) = 2 \lim_{z \rightarrow \infty} z \Phi_{1,2}(z).$$

Note that the independent variable x of the ODE enters the RHP as a parameter of the phase function θ : the RHP (with independent variable z) amounts thus for a *pointwise* evaluation of the Painlevé transcendent $u(x; s_1, s_2)$.

The numerical method of Olver. Olver (2011) constructed his spectral collocation method by recasting RHPs as a particular kind of singular integral equation. Upon writing

$$\Phi(z) = I + C_\Gamma U(z)$$

with the Cauchy transform of a matrix-valued function $U : \Gamma \rightarrow \operatorname{GL}(m, \mathbb{C})$, namely

$$C_\Gamma U(z) = \frac{1}{2\pi i} \int_\Gamma \frac{U(\zeta)}{\zeta - z} d\zeta,$$

the RHP becomes the linear operator equation

$$AU(z) = U(z) - C_\Gamma^{-1} U(z) \cdot (G(z) - I) = G(z) - I. \quad (1)$$

Here, $C_{\Gamma}^{\pm}U(z)$ denotes the non-tangential limit of $C_{\Gamma}U(z')$ as $z' \rightarrow z$ from the positive (negative) side of the contour; there is the operator identity $C_{\Gamma}^{+} - C_{\Gamma}^{-} = I$. The residue at ∞ becomes simply the integral

$$\operatorname{res}_{z=\infty} \Phi(z) = \frac{1}{2\pi i} \int_{\Gamma} U(\zeta) d\zeta.$$

Without going into details, in this paper it suffices to note that the n -point numerical approximation of (1) yields a finite-dimensional linear system

$$A_n U_n = b_n$$

where the j th component of the solution U_n is a matrix that approximates $U(z_j)$ at the collocation point $z_j \in \Gamma$ ($j = 1, \dots, n$). The stability of the method is essentially described by the condition number

$$\kappa_n = \kappa(A_n) = \|A_n^{-1}\| \cdot \|A_n\|$$

of this linear system: altogether, one would typically suffer a loss of $\log_{10} \kappa$ significant digits. Under an additional assumption, which can be checked *a posteriori* within the numerical method itself, Olver and Trogdon (2012, Assumpt. 6.1 and Lemma 6.1) proved a bound of the form²

$$\kappa_n = O(\kappa(A))$$

in terms of the condition number $\kappa(A) = \|A^{-1}\| \cdot \|A\|$ of the continuous operator A , with constants that are mildly growing in the number of collocation points n . Here, the operator norm of A is obtained by acting on $L^2(\Gamma)$. Extending U_n to all of Γ by interpolation, Olver and Trogdon (2012, Eq. (6.1)) also state an error estimate of the form

$$\|U - U_n\|_{L^2(\Gamma)} \leq c\kappa(A)n^{2+\beta-k}\|U\|_{H^k(\Gamma)}$$

with some $\beta > 0$. Since, for jump matrices G that are piecewise restrictions of entire functions, k can be chosen arbitrarily large, one gets spectral accuracy.

Preconditioning of RHPs. Thus, stability and accuracy of the numerical method depend on $\kappa(A)$, which blows up in many problems of interest. For instance, the undeformed version of the RHP for Painlevé II with the contours in Fig. 1 has $\kappa_n \approx 2.2 \cdot 10^8$ for $s_1 = 1$ and $s_2 = 2$ and $x = -10$ (see also Fig. 2 for varying x).

Now, it is important to understand that $\kappa(A)$ is the condition number of the RHP for the restricted data (Γ, G) but not for the jump data G_j ($j = 1, \dots, k$) which are obtained from analytic continuation. If the continued data are *explicitly* given, and are not themselves part of the computational problem,³ it should be possible to deform the RHP to an equivalent one with data $(\tilde{\Gamma}, \tilde{G})$ and

$$\kappa(\tilde{A}) \ll \kappa(A).$$

We call such a deformation a *preconditioning* one. In fact, Olver and Trogdon (2012) argued that preconditioning is possible whenever the method of nonlinear steepest descent produces an asymptotic formula; Fig. 4 shows a typical sequence of such manually constructed preconditioning deformations for the Painlevé II RHP.

²They employ the estimate $\|A\| \leq \sqrt{2}(1 + \|G - I\|_{L^\infty(\Gamma)}\|C_{\Gamma}^{-}\|)$ in their statements.

³Analytic continuation corresponds to solving a Cauchy problem for the elliptic Cauchy–Riemann differential equations; it is, therefore, an ill-posed problem.

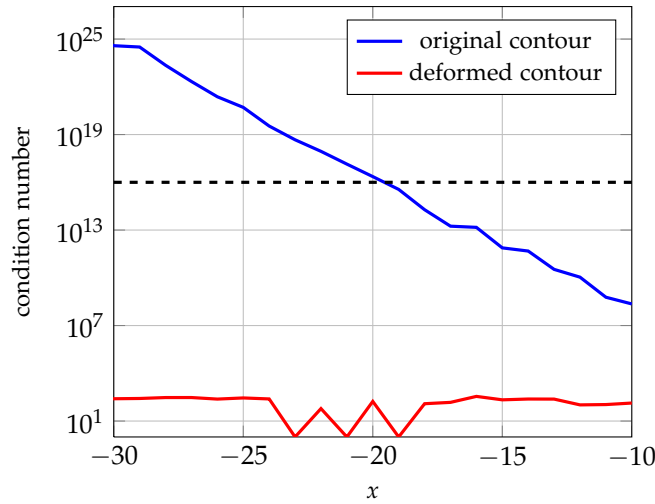


FIGURE 2. Comparison of the condition number of the original contour and of a deformed contour optimized by the greedy algorithm of §3 for the Painlevé II RHP with $(s_1, s_2) = (1, 2)$. The condition number of the deformed contour is roughly constant for all values of x while the condition number of the original contour grows exponentially fast for decreasing values of x . Note that condition numbers larger than 10^{16} (dashed line) obstruct the computation of even a single accurate digit in machine arithmetic, indicating severe numerical instability.

Though it seems to be difficult to extract a single governing principle for all the ingenious deformations that are used in the asymptotic analysis of RHPs, we base our algorithmic approach on the following simple observation: if there are no jumps in the RHP, that is if $G \equiv I$, we have $A = I$ and therefore $\kappa(A) = 1$. By continuity, $G \rightarrow I$ in some sufficiently strong norm would certainly imply $\kappa(A) \rightarrow 1$, such that a reasonably small $\|G - I\|$ will probably yield a moderately sized condition number $\kappa(A)$. We conjecture that such an estimate can be cast in the form

$$\kappa(A) \leq \phi(\|G - I\|_{W^{s,p}(\Gamma)})$$

for some Sobolev $W^{s,p}$ -norm and some monotone function ϕ that is independent of (Γ, G) . A good preconditioning strategy would then be to make $\|G - I\|_{W^{s,p}(\Gamma)}$ as small as possible, we call it the *relative strength* of the jump matrix G .

In the lack of any better understanding of the precise dependence of $\kappa(A)$ on the RHP data (Γ, G) we suggest to use $\|G - I\|_{L^1(\Gamma)}$ as a measure of relative strength: optimizing it led to significant reductions of the condition number in all of our experiments. However, the deformation algorithm itself will just use that the measure $d(\Gamma; G)$ can be written as an integral over Γ , namely in the form

$$d(\Gamma; G) = \int_{\Gamma} d(G(z)) d|z|$$

for some function $d : GL(m, \mathbb{C}) \rightarrow [0, \infty)$, which we call the *local weight*.

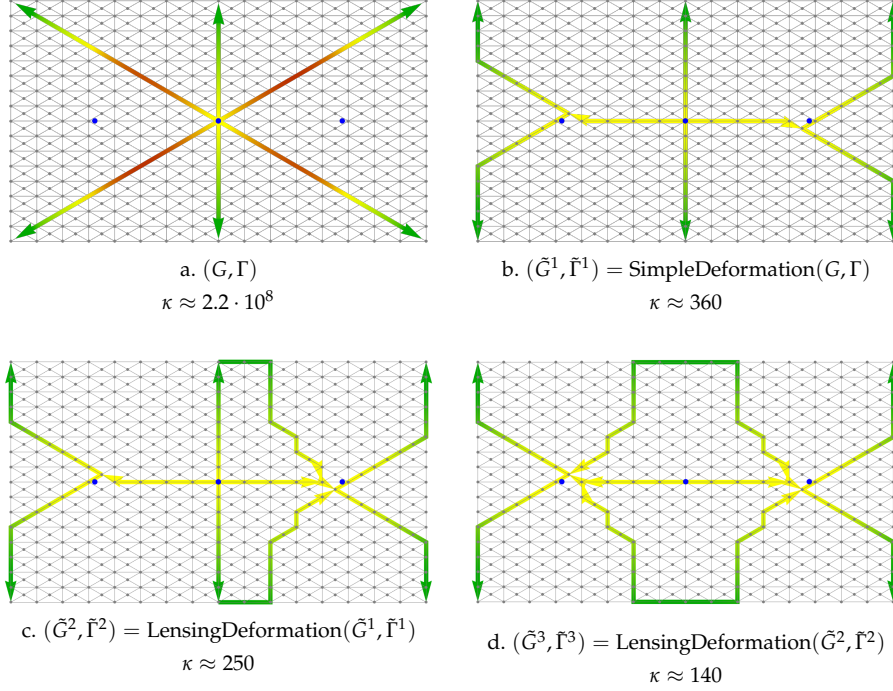


FIGURE 3. Application of SIMPLEDEFORMATION and LENSINGDEFORMATION of §3 to the Painlevé II RHP with $s_1 = 1$, $s_2 = 2$ and $x = -10$. On the top left is the original contour of this RHP and the other contours are deformed versions of it. All contours have been calculated on a 17×17 grid. The color encodes the magnitude of $\|G(z) - I\|_F$, with green = 10^{-16} , yellow = 1, and red = 10^4 . The blue dots indicate the origin $z = 0$ and the stationary points of the phase function θ at $z = \pm\sqrt{-x}/2$. The reduction of the condition number from (a) to (d) corresponds to an accuracy gain of about six digits.

Preconditioning as a discrete optimization problem. Since our objective is preconditioning, the relative strength of the jump matrices does not really have to be minimized over all equivalent deformations $(\tilde{\Gamma}, \tilde{G})$ of a given RHP (Γ, G) . For all practical purposes it suffices to consider just a very coarse, finite set of possible contours, namely paths within a planar graph.

The basic idea is as follows: first, we restrict the problem to a bounded region of the complex plane and embed the part of the contour Γ belonging to that region as paths into a coarse, grid-like planar graph $g = (V, E)$ (see Fig. 3.a for an example of the Painlevé II RHP: because of a super exponential decay as $z \rightarrow \infty$ along each of the rays, $G - I$ is already a computer zero outside the indicated rectangle).

Second, for each j , the analytic continuation G_j of the jump data on Γ_j turns the graph g into an edge-weighted graph g_j by using the (edge) weights

$$d_j(e) = \int_e d(G_j(z)) d|z| \quad (e \in E).$$

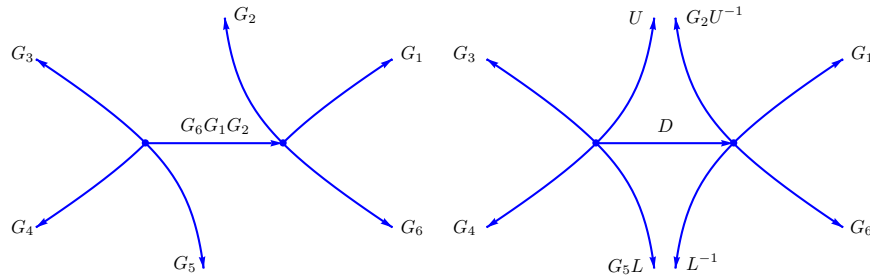


FIGURE 4. Some manual constructions for the Painlevé II RHP taken from Olver and Trogdon (2012, p. 20). Left: Deformation along the paths of steepest descent; right: deformation after lensing. The contours bifurcate at the stationary points of the phase function θ .

Last, we replace Γ_j (within the bounded domain) by the *shortest* path (with the same endpoints as Γ_j) with respect to g_j subject to the following constraint: the thus deformed RHP must be equivalent to the original one.

It is this latter constraint which adds to the algorithmic difficulty of the problem: the Γ_j cannot be optimized independent of each other. We will address this problem by a greedy strategy: the largest contribution to the weight constrains the admissible paths of the second largest one and so on; this will be accomplished by modifying the underlying graphs g_j in the corresponding order.

Fig. 3.b shows the result of such an algorithmic deformation for the Painlevé II RHP ($s_1 = 1$, $s_2 = 2$, $x = -10$): the condition number is reduced by about six orders of magnitude. Further improvement is possible by performing a “lensing” deformation, that is, by introducing multiple edges based on a factorization of G (see §3.3). The results of two such steps are shown in Fig. 3.c and d (more steps would not pay off). Though the improvement of the condition number is more modest in these two steps, it is instructive to compare the algorithmic contour in Fig. 3.d with the manual construction of Olver and Trogdon (2012) shown in Fig. 4.

Fig. 2 compares, for varying values of x , the condition number of the original contour with that of the deformed contour optimized by the greedy algorithm of §3: a uniform stabilization by preconditioning is clearly visible.

Outline of the paper. In §2 we discuss the two admissible deformations of RHPs that will be considered in this paper: simple deformations of contours and lensing deformations based on factorizations of the jump matrix G . We address the question of how to match the topological constraints of such deformations in the planar graphs attached to each part Γ_j of the contour. In §3 we give an in-depth description (with pseudo code) of the greedy algorithm that aims at optimizing these deformations. Important steps are illustrated for the Painlevé II RHP. Further details of the implementation are discussed in §4.

2. ADMISSIBLE DEFORMATIONS OF RIEMANN–HILBERT PROBLEMS

We briefly recall two of the deformations that can be applied to RHPs. A more detailed description can be found in Fokas et al. (2006).

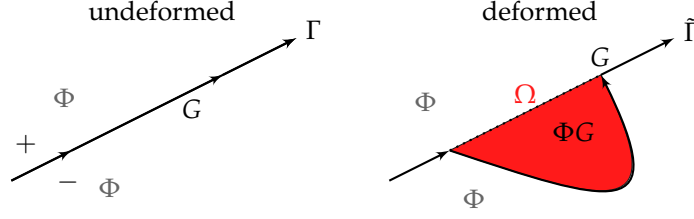


FIGURE 5. A simple deformation.

2.1. Simple Deformations. Fig. 5 shows an example of such a deformation. In general, simple deformations allow to continuously move a contour part in the complex plane (thereby covering a region Ω) as long as the following conditions are satisfied:

- (i) $\tilde{\Gamma}$ does not cross other parts of Γ ,
- (ii) Ω does not contain any other contour parts,
- (iii) G has a holomorphic continuation in Ω .

Then, the deformed RHP in Fig. 5 is solved by the function

$$\tilde{\Phi} = \begin{cases} \Phi G & : x \in \Omega, \\ \Phi & : x \notin \Omega. \end{cases}$$

Conditions (i)-(iii) can be mapped to graph-constrained deformations as follows:

Condition (i) can be handled by *splitting* a graph as shown in Fig. 6: if a path p corresponding to a part of a contour is given, like the path highlighted in blue, we duplicate the vertices of p and change all edges on the right side of p so that they are connected to the newly created vertices but not to the vertices of p itself. This way no path in the graph can cross p anymore. We will use $g[p_1, p_2, \dots]$ to denote a graph g which has been split in this fashion along the paths p_1, p_2, \dots .

Condition (ii) is difficult to be built into the structure of a graph *a priori*, but it is easy to check for it *a posteriori*: the circle composed by Γ_i and $\tilde{\Gamma}_i$ should not enclose an endpoint of another arc. If violated, the algorithm simply stops (this never happened in our experiments; dealing with such a situation would require to break the deformations into smaller pieces).

Condition (iii) can be handled by removing those regions from the graph where G does not have a holomorphic continuation.

2.2. Multiple Deformations and Factorization: Lensing. Fig. 7 shows an example of such a deformation. To initialize, several copies of a contour part are created at one and the same location, where each copy corresponds to a factor of a given multiplicative decomposition of the jump matrix G . We call these copies the *factors* of this part of the contour Γ . These factors are then moved around in the complex plane subject to conditions (i)-(iii) and, additionally, the following condition:

- (iv) the mutual orientation of the factors must be preserved.

For example, in Fig. 7 the order of the decomposition $G = LDU$ requires that the factor U is to the left of the factor D and that the factor D is to the left of the

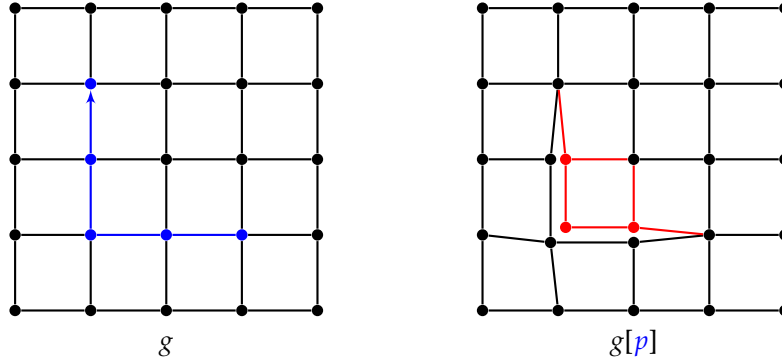


FIGURE 6. Illustration of split graphs. On the left side is the original graph g with a path p (highlighted in blue) along which it is about to be split. The split graph $g[p]$ is on the right side, with all vertices and edges that have been changed or created highlighted in red. For a clear visualization the split in the graph has been enlarged by moving the vertex positions; in the actual graphs used by the algorithm the duplicated vertices stay at exactly the same position. All graphs are undirected, the arrow at the end of the blue path just indicates its orientation.

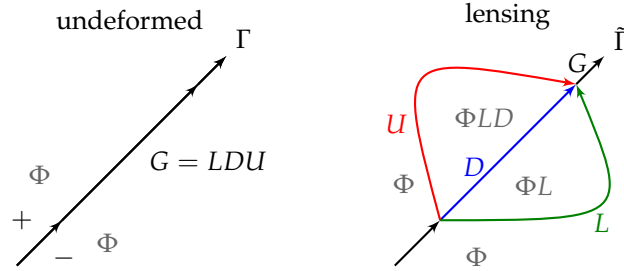


FIGURE 7. A lensing deformation.

factor L . To preserve this orientation in our deformation algorithm, we calculate the shortest path for just one of the factors. For the other factors we use a modification of the shortest enclosing circle algorithm of Provan (1989), see §3.3.

3. THE GREEDY ALGORITHM

3.1. Notation.

- d_e : weight of the edge e
- $P_1 \dot{+} P_2$: path P_1 joined with path P_2
- \overleftarrow{P} : reversed path P
- $P[u, v]$: subpath from vertex u to vertex v within the path P
- $\text{sp}(g, u, v)$: shortest path from vertex u to v in the weighted graph g
- $\text{int}(W)$: interior of a walk, that is, all vertices v with $\text{ind}(W, v) = \pm 1$
- p_- / p_+ : path on the left/right side of the split along p in $g[p]$

Algorithm 1 Optimized Simple Deformation

```

1: procedure SIMPLEDEFORMATION( $G, \Gamma$ )
2:    $n = |\Gamma|$  ▷  $n$  is the number of contour parts
3:    $P = ()$  ▷ fixed new paths
4:    $p = ()$  ▷ candidates for new paths
5:    $F = ()$  ▷ already processed contour parts
6:    $Q = (1, \dots, n)$  ▷ unprocessed contour parts
7:    $g = ()$  ▷ graphs corresponding to contour parts
8:    $g^* = ()$  ▷ initial not split graphs
9:   for all  $i \in Q$  do
10:      $g_i =$  graph with edge weights  $d_e = \|G_i - I\|_{L^1(e)}$ 
11:      $v_i^l =$  vertex in  $g_i$  nearest to left endpoint of  $\Gamma_i$ 
12:      $v_i^r =$  vertex in  $g_i$  nearest to right endpoint of  $\Gamma_i$ 
13:   end for
14:    $g^* = g$ 
15:   while  $Q \neq ()$  do
16:     for all  $i \in Q$  do
17:        $p_i = \text{sp}(g_i, v_i^l, v_i^r)$  ▷ shortest path from  $v_i^l$  to  $v_i^r$  in  $g_i$ 
18:     end for
19:      $i_* = \underset{i \in Q}{\text{argmax}} d(p_i)$ 
20:      $P_{i_*} = p_{i_*}$ 
21:      $Q = Q \setminus (i_*)$ 
22:     for all  $i \in F$  do ▷ try to improve the path if there is an intersection
23:       if  $P_{i_*} \cap P_i \neq \emptyset$  then
24:          $P = \text{ImproveSharedSubpath}(g^*, G, P, i, i_*)$ 
25:       end if
26:     end for
27:      $F = F \cup (i_*)$ 
28:     for all  $i \in Q$  do
29:        $g_i = g_i^*[P]$ 
30:     end for
31:   end while
32:    $(\tilde{G}, \tilde{\Gamma}) = \text{MapToRHP}(G, P)$  ▷ create new contour parts
33:   return  $(\tilde{G}, \tilde{\Gamma})$ 
34: end procedure

```

3.2. Optimized Simple Deformations. The idea of Algorithm 1 goes as follows: first (lines 9–13), for each of the contour parts Γ_j and the corresponding jump matrices G_j (which are assumed to have a holomorphic continuation to the rectangular region supporting the grid), a separate weighted graph g_j with edge weights

$$d_e = \int_e d(G_j(z)) d|z|$$

is created, see Fig. 8. Second (lines 16–18), each Γ_j is replaced by a shortest path that shares the same endpoints, see Fig. 9. The thus separately optimized paths, however, will in general not satisfy condition (i) of §2, that is, they will cross each

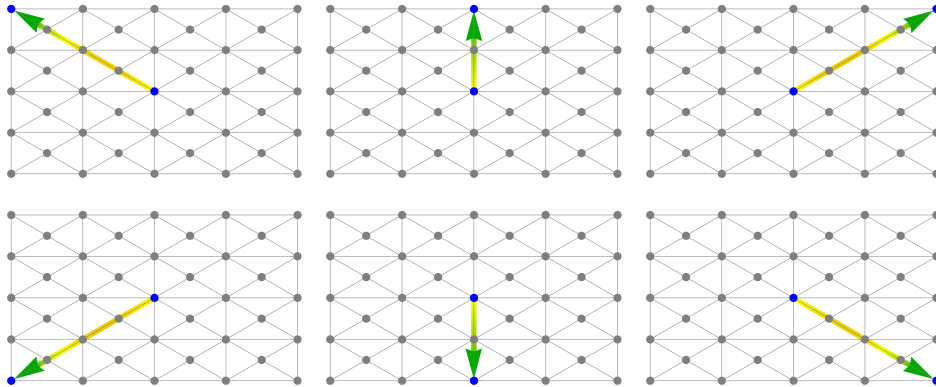


FIGURE 8. Create separate weighted graphs for each contour part Γ_j with weights depending on the jump matrix G_j (line 10 in Algorithm 1).

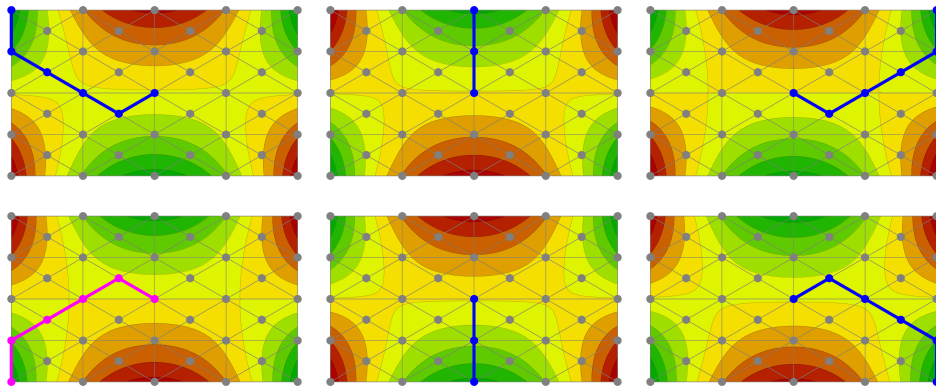


FIGURE 9. Calculate the shortest paths for each G_j separately, highlighted in blue (line 17 in Algorithm 1). The one with the largest total weight is shown in magenta (line 19). The color encodes the magnitude of $\|G_j(z) - I\|_F$, with green = 10^{-16} , yellow = 1, and red= 10^{16} .

other. Therefore, some of the paths have to be modified to match this condition, which increases the corresponding weight. By keeping, third (lines 19–20), the path P of dominant total weight fixed, we restrict such modifications to the other parts that contribute less to the condition number. By splitting, fourth (lines 28–29), all graphs along P and repeating (lines 16–18) the calculation of the shortest paths in the split graphs, we come up with paths that do not cross P , see Fig. 10.

This procedure is then repeated, fifth (line 15), until all paths are fixed and, hence, non-crossing. (In each round of this loop another path gets fixed.) Finally, sixth (line 32), the algorithm constructs the deformed contour data from the just calculated set of paths. For paths and subpaths that do not share an edge with another path we simply use the path and the corresponding jump matrix as new contour data. Subpaths which occur in more than one path will be mapped to new contour data by performing an “inverse lensing”: the new jump matrix is

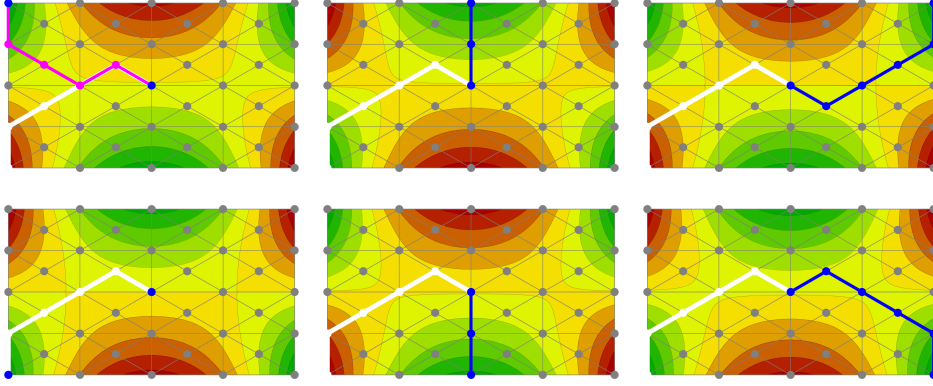


FIGURE 10. Recalculate the shortest paths (line 17 in Algorithm 1) in the graphs split along the optimal path of largest weight from Fig. 9, here shown in white. The new shortest paths are highlighted in blue, the one of maximal weight in magenta.

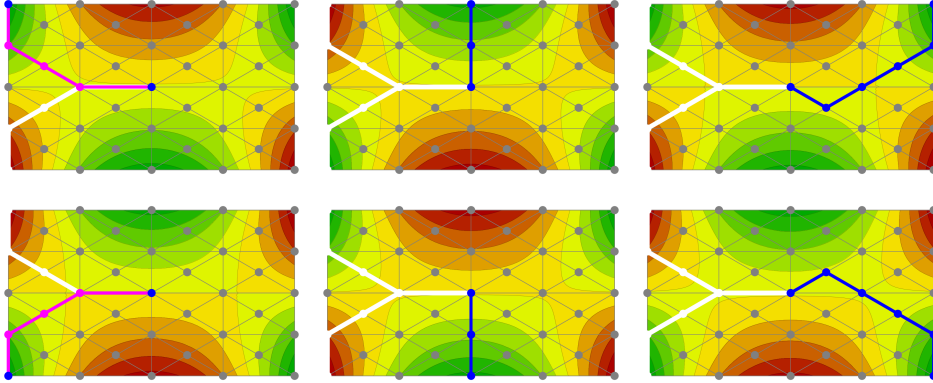


FIGURE 11. Improvement of the subpath shared by the fixed white path and the magenta path of Fig. 10 (Algorithm 2). After this improvement, both paths are fixed and the graphs are split along their union (the white Y-shape contour). From here it should be clear, how Algorithm 1 arrives (for a finer grid) at the deformed contours shown in Fig. 3.b.

calculated as the (properly ordered) product of all the jump matrices sharing the that subpath. For example, if the paths P_i and P_j have a common subpath s and P_i is to the left of P_j , the procedure MAPToRHP creates a new contour part s with the jump matrix $G_j G_i$.

In a situation as shown in Fig. 10, where the new optimal paths share a subpath with the already fixed ones, further improvement is possible (lines 23–25) by optimizing the shared subpath with respect to the weight obtained from combining the corresponding jump matrices (that is, the just mentioned “inverse lensing”). This procedure (Algorithm 2) is schematically illustrated in Fig. 12; the application of this procedure to the example of Fig. 10 is shown in Fig. 11.

Algorithm 2 Improve Paths with a Shared Subpath

```

1: procedure IMPROVESHAREDSPATH( $g, G, P, i_1, i_2$ )
2:    $g' = g_{i_1}$  ▷ create a temporary graph
3:   if  $P_{i_1}$  left of  $P_{i_2}$  then
4:     set weights for edges  $e$  of  $g'$  to  $d(e) = \|G_{i_2}G_{i_1} - I\|_{L^1(e)}$ 
5:   end if
6:   if  $P_{i_1}$  right of  $P_{i_2}$  then
7:     set weights for edges  $e$  of  $g'$  to  $d(e) = \|G_{i_1}G_{i_2} - I\|_{L^1(e)}$ 
8:   end if
9:    $s = P_{i_1} \cap P_{i_2}$  ▷ split  $P_{i_1}$  and  $P_{i_2}$  into left,common and right subpath
10:   $(P_{i_1}^l, s, P_{i_1}^r) = P_{i_1}$ 
11:   $(P_{i_2}^l, s, P_{i_2}^r) = P_{i_2}$ 
12:   $P' = P \setminus \{P_{i_1}, P_{i_2}\}$ 
13:   $g' = g'[P', P_{i_1}^l \overset{\leftarrow}{+} P_{i_2}^l, P_{i_1}^r \overset{\leftarrow}{+} P_{i_2}^r]$ 
14:   $p_* = sp(g', s_1, s_{-1})$  ▷  $p_*$  = shortest path between start and end vertex of  $s$ 
15:   $P_{i_1} = P_{i_1}^l \cup p_* \cup P_{i_1}^r$ 
16:   $P_{i_2} = P_{i_2}^l \cup p_* \cup P_{i_2}^r$ 
17:  if containsCircle( $P_{i_1}$ ) then
18:     $P_{i_1} = \text{dropCircle}(P_{i_1})$ 
19:     $s = P_{i_1} \cap P_{i_2}$ 
20:     $P_{i_2} = sp(g_{i_2}[P \setminus P_{i_2}], (P_{i_2})_1, (P_{i_2})_{-1})$ 
21:    if  $P_{i_1} \cap P_{i_2} \neq s$  then
22:       $P = \text{ImproveSharedSubpath}(g, G, P, i_1, i_2)$ 
23:    end if
24:  else if containsCircle( $P_{i_2}$ ) then
25:     $P_{i_2} = \text{dropCircle}(P_{i_2})$ 
26:     $s = P_{i_1} \cap P_{i_2}$ 
27:     $P_{i_1} = sp(g_{i_1}[P \setminus P_{i_1}], (P_{i_1})_1, (P_{i_1})_{-1})$ 
28:    if  $P_{i_1} \cap P_{i_2} \neq s$  then
29:       $P = \text{ImproveSharedSubpath}(g, G, P, i_1, i_2)$ 
30:    end if
31:  end if
32:  return  $P$ 
33: end procedure

```

3.3. Optimized Lensing Deformations. A single step of the optimized lensing deformation (Algorithm 3) aims at improving the dominant part of the contour by trying various decompositions (factorizations) of its jump matrix to which, then, the optimized simple deformation (Algorithm 1) is applied. The contour parts which originate from such a lensing deformation (e.g. L , D and U in Fig. 7) have, however, to satisfy an additional constraint, namely condition (iv) of §2: their spatial order has to be preserved. To calculate shortest paths (line 17 in Algorithm 1) subject to this additional condition, we distinguish between the following three cases (an illustration can be found in Fig. 13):

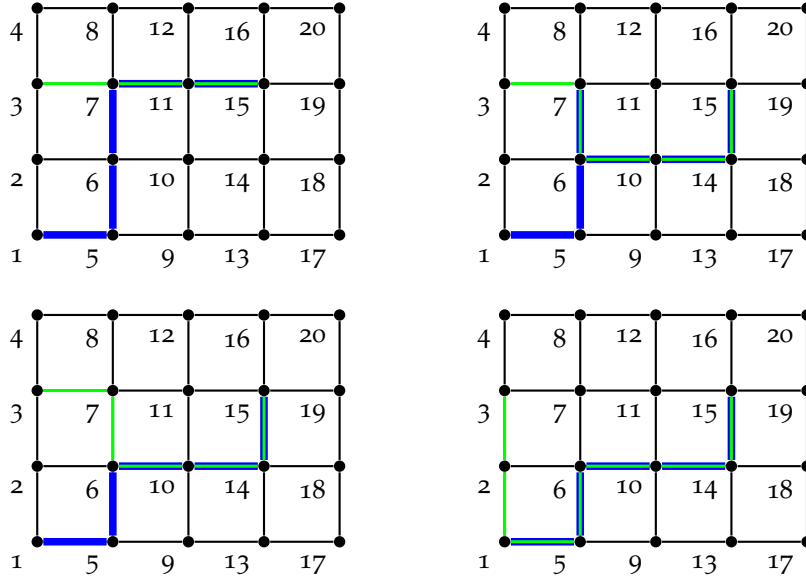


FIGURE 12. An illustration of applying one round of IMPROVESHARED-SUBPATH (Algorithm 2). Top left: a graph in which the two paths P_i and P_j shown in blue and green share the subpath $(7,11,15)$. Top right: after calculating a shortest path from 7 to 15 for the combined weight (lines 3–8 in Algorithm 2), the blue path contains the circle $(6,7,6)$. Bottom left: this circle gets removed from the blue path. Bottom right: an updated shortest green path results in a new shared subpath that could be further improved by applying IMPROVESHARED-SUBPATH recursively.

Algorithm 3 Optimized Lensing Deformation

```

1: procedure LENSINGDEFORMATION( $G, \Gamma$ )
2:   select  $\Gamma_j$  with highest weight
3:   for  $\mathcal{D} \in \{LDU, LR, \dots\}$  do
4:      $G^{\mathcal{D}} = (G_1, \dots, G_{j-1}, \text{decomposition } \mathcal{D} \text{ of } G_j, \dots, G_{j+1}, \dots, G_n)$ 
5:      $\Gamma^{\mathcal{D}} = (\Gamma_1, \dots, \Gamma_{j-1}, \underbrace{\Gamma_j, \Gamma_j, \Gamma_j, \dots, \Gamma_j, \Gamma_j, \Gamma_j}_{\# \text{ copies} = \# \text{ factors in } \mathcal{D}}, \Gamma_{j+1}, \dots, \Gamma_n)$ 
6:      $(\tilde{G}^{\mathcal{D}}, \tilde{\Gamma}^{\mathcal{D}}) = \text{SimpleDeformation}(G^{\mathcal{D}}, \Gamma^{\mathcal{D}})$ 
7:   end for
8:   return  $(\tilde{G}^{\mathcal{D}}, \tilde{\Gamma}^{\mathcal{D}})$  with lowest weight
9: end procedure

```

- Notation: T denotes the list of indices of the contour parts that are created by the decomposition and i denotes the index for which a shortest path is currently calculated. We recall that Q denotes the parts of the contour that have not yet been fixed in the course of Algorithm 1.

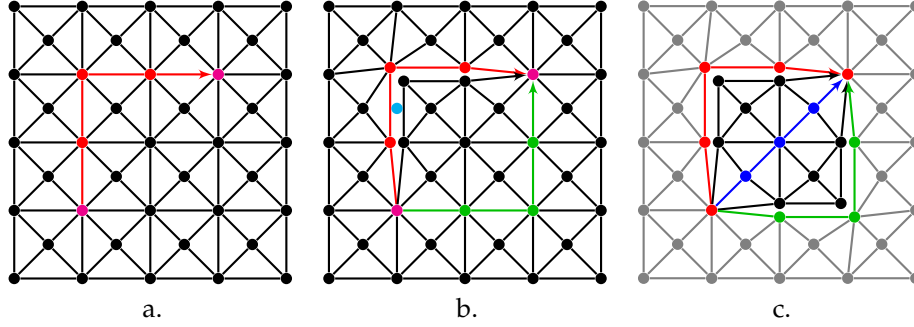


FIGURE 13. Illustration of the shortest path calculations done for a lensing deformation as in Fig. 7. Here, all three cases appear: **a.** All parts of the decomposition are still unprocessed (case 1). A shortest path p_i (red) has to be calculated between the endpoints (magenta) of Γ_i . **b.** A path P_l for the contour part Γ_l (red) to the left of Γ_i has already been fixed and the graph has been split accordingly (case 2). Now, p_i must be constructed as the shortest path subject to the constraint that the circle $p_i \dot{+} P_l$ encloses some point c in the split (shown in cyan). All edges are undirected, the arrows just indicate the directions of the paths. **c.** P_l (red) to the left side of p_i (blue) and P_r (green) to the right side of p_i have already been fixed and the graph split accordingly (case 3). All vertices that are removed from the graph before calculating the shortest path p_i are shown in gray.

- Case 1: $T \cap Q = T$.

As no path belonging to T has been fixed, there are no constraints yet to be observed and we can simply calculate the shortest path for i .

- Case 2: either $\exists l \in T \setminus Q$ with Γ_l left of Γ_i or $\exists r \in T \setminus Q$ with Γ_r right of Γ_i .

Without loss of generality, we assume that we have to construct a shortest path Γ_i subject to the constraint that it is to the right of an already fixed path P_l . Now, let c be a point that is located between the left and right side of the split in the graph g_i caused by P_l . Then, the order constraint is identical to finding the shortest path p_i for which the circle formed by joining p and P_l encloses c . Lemma 1, stated at the end of this section, will show that p_i is actually given by

$$\Pi = \{\text{sp}(g_i, v_i^l, u) \dot{+} uw \dot{+} \text{sp}(g_i, w, v_i^r) : uw \text{ edge in } g_i\},$$

$$p_i = \text{argmin}\{d(p) : p \in \Pi; \text{ind}(p \dot{+} P_l, c) = \pm 1\}.$$

Hence, p_i can be constructed by a minor modification of the polynomial algorithm for shortest enclosing circles in embedded graphs (Provan 1989).

- Case 3: $\exists l \in T \setminus Q$ with Γ_l left of Γ_i and $\exists r \in T \setminus Q$ with Γ_r right of Γ_i .

The shortest path for Γ_i , subject to the constraint that it is right of Γ_l and left of Γ_r , can only contain vertices inside the circle formed by joining P_l and P_r . Therefore, we construct p_i as the shortest path in a smaller graph, in which all vertices outside of this circle have been removed.

Lemma 1. Let $q = (q_1, \dots, q_n)$ be a path in a weighted planar graph $g = (V, E)$, let c be a point considered⁴ to be in the split along q in $g[q]$ and define

$$\Pi = \{\text{sp}(g[q], q_1, u) \dot{+} uv \dot{+} \text{sp}(g[q], v, q_n) : uv \in E\}.$$

Then the shortest walk p_* in g , subject to the constraint $\text{ind}(p_* \dot{+} \overleftarrow{q}, c) = \pm 1$, satisfies

$$p_* = \text{argmin}\{d(p) : p \in \Pi; \text{ind}(p \dot{+} \overleftarrow{q}, c) = \pm 1\}. \quad (2)$$

Proof. We restrict ourselves to the case $\text{ind}(p \dot{+} \overleftarrow{q}) = 1$, because the proof for the other case differs just in the sign of some winding numbers. We will assume to the contrary that p_* is not given by (2) and will get a contradiction.

If there is more than one shortest walk p_* , we choose the one which encloses the least number of vertices. If $p_* \notin \Pi$, then there has to be a vertex $v \in p_*$ with $p_* = l \dot{+} v \dot{+} r$ such that $s_l = \text{sp}(g[q], q_1, v)$ and $s_r = \text{sp}(g[q], v, q_n)$ satisfy the following conditions

$$\text{ind}(s_l \dot{+} r \dot{+} \overleftarrow{q}, c) \neq 1, \quad \text{ind}(l \dot{+} s_r \dot{+} \overleftarrow{q}, c) \neq 1. \quad (3)$$

We will now show that there is no such vertex v .

Step 1. To begin with, we prove for $W = p_* \dot{+} \overleftarrow{q}$ that

$$s_l \cap \text{int}(W) = \emptyset, \quad s_r \cap \text{int}(W) = \emptyset. \quad (4)$$

If (4) would not hold then either s_l or s_r contains a path $p = (p_1, \dots, p_m)$ with $p_2, \dots, p_{m-1} \in \text{int}(W)$ and $p_1, p_m \in p_*$. As s_l and s_r are shortest paths, such a subpath p has to be the shortest path from p_1 to p_m . Consequently, the walk

$$W' = p_*[q_1, p_1] \dot{+} p \dot{+} p_*[p_m, q_n] \dot{+} \overleftarrow{q}$$

would satisfy

$$d(W') \leq d(W), \quad \text{ind}(W', c) = 1, \quad |\text{int}(W')| < |\text{int}(W)|,$$

which contradicts our choice of p_* . Therefore, (4) holds.

Step 2. We now prove that

$$\begin{aligned} \text{ind}(W_1^l, c) = 1 & \quad \text{with } W_1^l = l \dot{+} \overleftarrow{s_l}, \\ \text{ind}(W_1^r, c) = 1 & \quad \text{with } W_1^r = r \dot{+} \overleftarrow{s_r}. \end{aligned} \quad (5)$$

To this end, we consider the walk

$$W^l = l \dot{+} \overleftarrow{s_l} \dot{+} s_l \dot{+} r \dot{+} \overleftarrow{q}$$

which consists of the two circles

$$W_1^l = l \dot{+} \overleftarrow{s_l}, \quad W_2^l = s_l \dot{+} r \dot{+} \overleftarrow{q},$$

and satisfies

$$\text{ind}(W, c) = \text{ind}(W^l, c) = \text{ind}(W_1^l, c') + \text{ind}(W_2^l, c') = 1. \quad (6)$$

If $s_l \cap W = \emptyset$, then neither W_1^l nor W_2^l contains any vertex more than once. As g is a planar graph, these walks correspond to simple closed curves in the complex

⁴We can chose any point on q for c and treat it as if it were right of q_- and left of q_+ .

plane and therefore their winding numbers around c can only be $-1, 0$ or 1 . If we also take (6) and (3) into account, the only possible option is

$$\text{ind}(W_1^l, c) = 1, \quad \text{ind}(W_2^l, c) = 0.$$

Unfortunately, $s_l \cap W = \emptyset$ does not necessarily have to be satisfied. But s_l cannot cross l and $r \dot{+} \overleftarrow{q}$ because of (4), which means that

$$s_l = \text{sp}(g[q], q_1, v) = \text{sp}(g[q, \overleftarrow{l}, q \dot{+} \overleftarrow{r}], q_1, v).$$

Hence, we can find the following walks in $g[q, \overleftarrow{l}, q \dot{+} \overleftarrow{r}]$

$$U_1^l = l_+ \dot{+} \overleftarrow{s}_l, \quad U_2^l = s_l \dot{+} r_+ \dot{+} \overleftarrow{q}_+,$$

which are equivalent to W_1^l and W_2^l but do not contain duplicate vertices. If we move the paths along the splits \overleftarrow{l} and $q \dot{+} \overleftarrow{r}$ a little bit apart, then U_1^l and U_2^l correspond to simple connected curves, too. As we can move the split paths apart without crossing c or any other part of U_1^l or U_2^l , these walks can only have winding numbers of $-1, 0$ or 1 with respect to c . This means that W_1^l and W_2^l can only have these winding numbers even if $s_l \cap W \neq \emptyset$. This proves the first relation in (5). The second one follows likewise.

Step 3. We claim that

$$\begin{aligned} q_n &\in \text{int}(W_1^l), & q_n &\notin \text{int}(W_1^r), \\ q_1 &\in \text{int}(W_1^r), & q_1 &\notin \text{int}(W_1^l). \end{aligned} \tag{7}$$

Combining (4) and (5) yields $\text{int}(W) \subseteq \text{int}(W_1^l)$. Therefore all vertices in W either have to be in $\text{int}(W_1^l)$ or in W_1^l . It follows that we just have to show that $q_n \notin W_1^l$. We consider the following closed walk

$$W' = W_1^l \dot{+} W_1^r = l \dot{+} r \dot{+} \overleftarrow{s}_r \dot{+} \overleftarrow{s}_l$$

with

$$\text{ind}(W') = \text{ind}(W_1^l) + \text{ind}(W_1^r) = 2.$$

If $q_n \in W_1^l$, then $s_l[q_n, v] = \overleftarrow{s}_r$ and, consequently, W' contains a circle that does not enclose any vertex. Removing this circle from W' results in the walk

$$W'' = l \dot{+} r \dot{+} \overleftarrow{s}_l[q_n, q_1]$$

without changing the winding number. So $\text{ind}(W'') = 2$, and the argument that we have used before to show $\text{ind}(W_1^l, c) \in \{-1, 0, 1\}$ works for W'' , too. Consequently, we get $q_n \notin W_1^l$. The second claim in (7) follows likewise.

Step 4. (see Fig. 14) We combine the results of the previous steps to show that our initial assumption leads to a contradiction. As $c \in \text{int}(W_1^l) \cap \text{int}(W_1^r)$ by (5), the two circles W_1^l and W_1^r have a non empty intersection. Furthermore, because of (7), none of them is completely contained within the other. It follows that W_1^l and W_1^r have to cross each other at two or more points. One of these can be v , but there is actually no other vertex at which the circles could cross: s_l cannot cross r and, vice versa, s_r cannot cross l due to (4); also s_l and s_r cannot cross because they are both shortest paths. \square

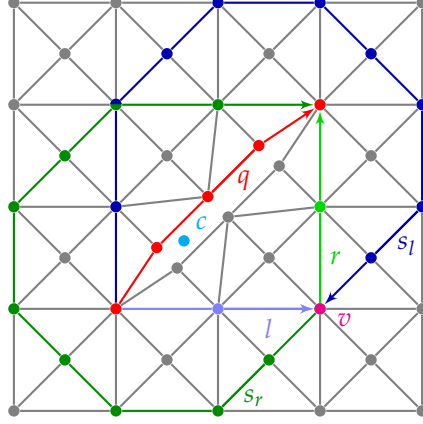


FIGURE 14. Illustration of Step 4 in the proof of Lemma 1.

4. IMPLEMENTATION DETAILS

4.1. **The Weights.** The weight d_e of an edge e should be an approximation of

$$\int_e \|G(z) - I\| d|z|$$

with a suitable matrix norm. Our experiments indicate that we generally need fewer collocation points if we aim at minimizing all components of $G - I$ instead of just focussing on its largest component, for which reason we choose the Frobenius (or Hilbert-Schmidt) norm. The integral is sufficiently well approximated by the two point trapezoidal quadrature rule (we recall that the aim of optimizing the weight is just preconditioning, that is, getting a particular good *order of magnitude* of the condition number). We thus take

$$d_e = \frac{1}{2} |b - a| (\|G(b) - I\|_F + \|G(a) - I\|_F)$$

as the weight of an edge e with the endpoints a and b .

4.2. **The Graph.** The algorithm of §3 is based on *planar* graphs. If the graph were not planar, paths could cross each other even without having any vertices in common and, therefore, the graph splitting described in §2 would not ensure that paths calculated by Algorithm 1 do not cross. We choose planar graphs built from rectangular grids to which a vertex in the center of each box is added that is connected to the vertices of the that box. Such a graph is chosen to subdivide a rectangle that contains all finite endpoints of Γ . We take this rectangle large enough so that outside of it $\|G - I\|_F$ is below machine precision on all arcs with an infinite endpoint, see Fig. 15. For numerical purposes, the jump matrix G is then indistinguishable from the identity matrix in the exterior of this rectangle: the RHP needs only to be solved in the interior.

4.3. **Contour Simplification.** The algorithm described in §3 returns a contour composed of a set of paths in the underlying graph. The collocation method of Olver (2011), which is finally employed for the numerical solution of the RHP,

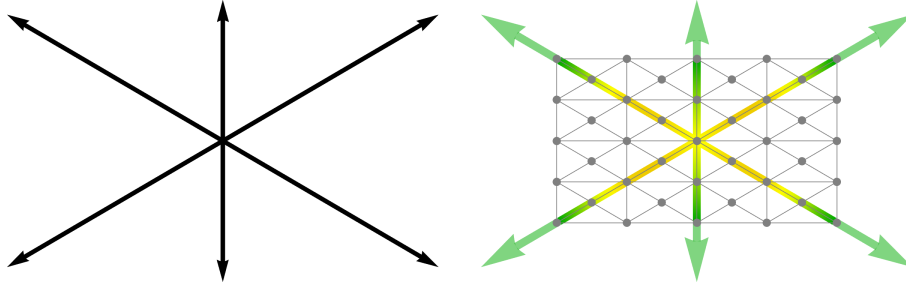


FIGURE 15. The rectangle to be covered by the grid is determined by the condition $\|G - I\|_F > 10^{-16}$ along Γ . The color coding is as in Fig. 3.

would have to place individual Chebyshev points on each smooth (that is, linear) part of this piecewise linear contour. For efficiency reasons it would thus be preferable to have a contour with fewer breakpoints. Consequently, for each optimized path, we calculate a coarse piecewise linear approximation that has about the same weight. Quite often just a straight line connecting the endpoints of a path is already sufficient approximation. Fig. 16 shows an example of this simplification process when applied to the final contour of Fig. 3: it cuts the number of collocation points by more than a factor of two while keeping the order of magnitude of the condition number constant.

CONCLUSION

The numerical results of this paper show that our algorithm can significantly reduce the condition number of RHPs. As a feature, this algorithm does not require any input, or knowledge, from the user other than the RHP at hand. Besides being thus a very convenient tool for the numerical solution of RHPs, the deformations automatically constructed by this algorithm might even turn out to be useful for determining first drafts of suitable deformations in the analytic study of RHPs.

Acknowledgement. This research was supported by the German Research Foundation (DFG), Collaborative Research Center SFB-TR 109.

REFERENCES

- Bornemann, F. and Wechsberger, G.: 2012, Optimal contours for high-order derivatives, *IMA J. Numer. Anal.* (to appear). e-print: [arXiv:1107.0498v2](https://arxiv.org/abs/1107.0498v2).
- Deift, P. A.: 1999, *Orthogonal polynomials and random matrices: a Riemann-Hilbert approach*, American Mathematical Society, Providence, RI.
- Deift, P. and Zhou, X.: 1993, A steepest descent method for oscillatory Riemann–Hilbert problems: Asymptotics for the MKdV equation, *Ann. of Math.* **137**, 295–368.
- Fokas, A. S., Its, A. R., Kapaev, A. A. and Novokshenov, V. Y.: 2006, *Painlevé Transcendents: The Riemann-Hilbert Approach*, American Mathematical Society, Providence, RI.
- Its, A. R.: 2003, The Riemann–Hilbert problem and integrable systems, *Notices Amer. Math. Soc.* **50**, 1389–1400.
- Olver, S.: 2011, Numerical solution of Riemann-Hilbert problems: Painlevé II, *Found. Comput. Math.* **11**, 153–179.

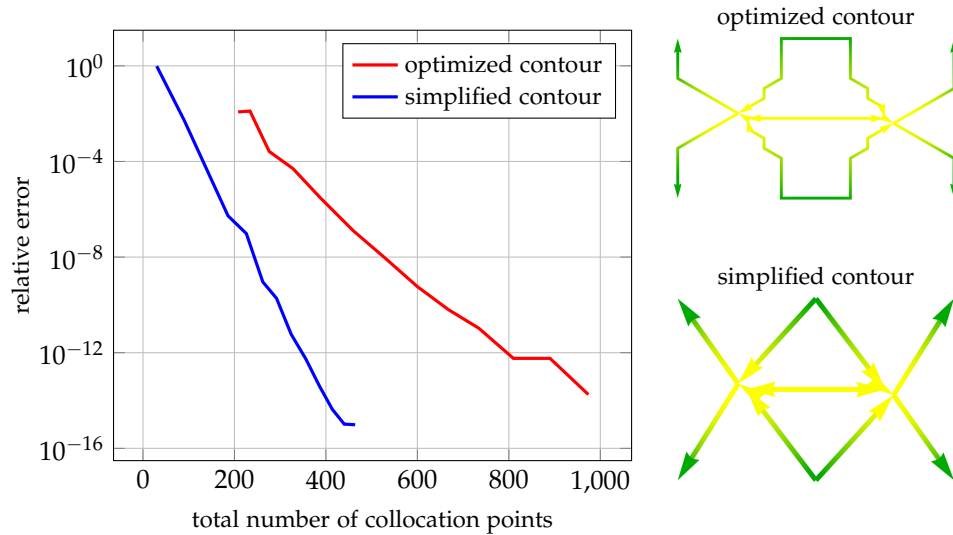


FIGURE 16. Improvement of the convergence rate by contour simplification: the simplified contour needs only about half the number of collocation points to reach the same accuracy as the optimized contour of Fig. 3.d (the color coding is the same as there). This simplification does not, however, worsen the order of magnitude of the condition number which grows from about 140 to just about 200. The similarity with the manually constructed contour in Fig. 4 is even more striking after this simplification step.

Olver, S. and Trogdon, T.: 2012, Nonlinear steepest descent and the numerical solution of Riemann–Hilbert problems. e-print: [arXiv:1205.5604](https://arxiv.org/abs/1205.5604).

Provan, J. S.: 1989, Shortest enclosing walks and cycles in embedded graphs, *Inform. Process. Lett.* **30**, 119–125.

ZENTRUM MATHEMATIK – M₃, TECHNISCHE UNIVERSITÄT MÜNCHEN, 80290 MÜNCHEN, GERMANY
E-mail address: wechslbe@ma.tum.de

ZENTRUM MATHEMATIK – M₃, TECHNISCHE UNIVERSITÄT MÜNCHEN, 80290 MÜNCHEN, GERMANY
E-mail address: bornemann@tum.de